Available online at www.sciencedirect.com
ScienceDirect
International Journal of Heat and Mass Transfer 51 (2008) 283–293
International Journal of HEAT and MASS TRANSFER
www.elsevier.com/locate/ijhmt

Free convective heat transfer in an enclosure with an internal louvered blind

T. Avedissian, D. Naylor *

Department of Mechanical and Industrial Engineering, 350 Victoria Street, Ryerson University, Toronto, Ontario, Canada M5B 2K3

Received 1 December 2006; received in revised form 30 March 2007
Available online 13 June 2007

Abstract

A numerical study has been conducted of free convection in a tall vertical enclosure with an internal louvered metal blind. The study considers the effects of Rayleigh number, enclosure aspect ratio, and blind geometry on the convective heat transfer. The numerical model has been validated against experimental measurements and the results have been presented in terms of an empirical correlation for the average Nusselt number. The correlation is applicable to an enclosure with an internal metal blind. It has been shown that the Nusselt number correlation can be combined with a simple one-dimensional model to closely predict the enclosure *U*-value.

Keywords: Free convection; Numerical simulation; Fenestration; Louvers; Blind; Correlation

1. Introduction

Software based on one-dimensional heat transfer models is widely used for the design and rating of fenestration. For example, in the United States the National Fenestration Rating Council specifies the use of a program called WINDOW [1] as part of its procedure for determining the overall *U*-value of a window [2]. The Canadian Standard A440.2-98 [3] on fenestration thermal performance specifies a similar program, VISION [4]. These programs use empirical correlations for the convective heat transfer and standard gray-diffuse analysis for thermal radiation.

Heat transfer models for unshaded glazing configurations are well-established and have been validated experimentally. In contrast, much less research has been done to develop reliable models for so-called "complex fenestration", which include the effect of common shading devices. Shades such as drapes, louvered blinds, and roller blinds interact with the convective flow and act as a shield to thermal radiation. Some recent studies have shown that they can have a substantial effect on the *U*-value of a window [5–7].

The current study considers the heat transfer in a double glazed window with a set of horizontal metal louvers located between the panes. This type of window-integrated shading is widely available in the North American residential consumer market. Also, this configuration is of special interest for use in "intelligent" building schemes. When motorized, a louvered blind can be an economical way to achieve a "switchable" glazing for the control of solar heat gain. The result can be a reduction in the energy requirements for winter heating, summer cooling and interior lighting [8–10].

There have been several previous numerical studies of free convection in a tall enclosure with an internal blind. Zhang et al. [11] have studied natural convection in a vertical enclosure with a permeable screen, similar to the louvered blind considered in the present study. However, the main focus of this study was on the permeability of a blind near the closed position. Garnet [12] developed a finite-volume CFD model of an enclosure with 34 between-pane

* Corresponding author. Tel.: +1 416 979 5000x6428; fax: +1 416 979 5265.
E-mail address: dnaylor@ryerson.ca (D. Naylor).

0017-9310/$ - see front matter © 2007 Elsevier Ltd. All rights reserved.
doi:10.1016/j.ijheatmasstransfer.2007.03.042

Nomenclature

A	enclosure aspect ratio, H_C/W_C
C_B	blind curvature
c_p	fluid specific heat
$F_{k,j}$	radiation view factor from surface k to j
Gr	Grashof number
g	acceleration due to gravity
H_C	enclosure height
$\bar{h}$	average convective heat transfer coefficient
J	radiosity
k	thermal conductivity
Nu_{W_C}	local Nusselt number
$\overline{Nu}_{W_C}$	average Nusselt number
P	dimensionless pressure defect
p	pressure defect
Pr	Prandtl number
q	convective heat transfer rate per unit depth
q''	convective heat flux
Ra_{W_C}	Rayleigh number based on the enclosure width, W_C
Ra_{W^*}	Rayleigh number based on the blended width, W^*
S	slat pitch
T	temperature
T^*	dimensionless temperature
t_B	slat thickness
U-value	overall thermal conductance of the window/blind system
U, V	dimensionless X, Y fluid velocities
u, v	x, y fluid velocities
W	width
W^*	blended width for correlation
X, Y	dimensionless Cartesian coordinates
x, y	Cartesian coordinates

Greek symbols

α	fluid thermal diffusivity
β	volumetric expansion coefficient
ε	emissivity
ϕ	slat angle
μ	fluid dynamic viscosity
ρ	fluid density
σ	Stefan–Boltzmann constant

Subscripts

B	blind
C	cold wall or cavity
cond	conduction
encl	overall enclosure
f	fluid
H	hot wall
rad	radiation

aluminum louvers. However, severe convergence problems were encountered and only a limited set of results were obtained for the slats in the horizontal position. More recently, Dalal [13] has used CFD to study the effect of a paper or cloth pleated blind on the convection and radiation inside a tall window. The results suggest that a between-panes blind can significantly improve the thermal resistance of a window, since it inhibits free convection and provides shielding to thermal radiation.

Recently, experimental measurements of the heat transfer through a double glazed window with a between-panes blind have been made by Huang [14] and Naylor and Lai [15]. Both studies used a commercial aluminum blind with horizontal louvers, i.e., a venetian-type blind. Huang [14] used a guarded heater plate apparatus to obtain U-value measurements at several slat angles and glazing spacings, with air as the fill gas. Naylor and Lai [15] used a laser interferometer to obtain temperature field visualization and detailed local Nusselt number data. The results from these experimental studies will be used to validate the present numerical solution.

Several other researchers have also considered the effects of louvers on the heat transfer in various window and window-like geometries. Safer et al. [16] have modeled the air flow in a double-skin facade equipped with a horizontal venetian blind and forced ventilation. The study examined the effect of slat angle, blind position and air outlet position on the velocity profiles in the double-skin facade. Fang [17] used a guarded hot box apparatus to measure the effect of a low emissivity louvered blind on the U-value of a single and double glazed window, with the blind mounted on the indoor and outdoor sides of the window. Scozia and Frederick [18] obtained numerical solutions for natural convection in slender window-like cavity containing air, with conducting fins attached to the cold wall. They considered the effect of enclosure aspect ratio, enclosure inclination angle and fin length on the average Nusselt number. Other studies have examined the effect of louvered blinds on the solar heat gain through a shaded window [19,20].

In the current study, a CFD model is developed of the conjugate heat transfer in a double glazed window with a between panes blind. The results of this parametric study are used to generate an empirical correlation for the average Nusselt number, which is needed for use in simplified models. Sample results are presented to illustrate the accuracy of a simplified one-dimensional analysis, which would be suitable for incorporation into existing window thermal analysis programs. It should be noted that the current work considers only the case where there is no solar heating of the blind, i.e. no insolation.

2. Governing equations and solution procedure

Fig. 1 shows the problem geometry and coordinate system for the present numerical solution. A louvered blind is located centrally between the panes of a tall double glazed window. The window glazings and end walls form a vertical enclosure of width W_C and height H_C. The glazing surfaces are approximated as isothermal and the end walls are assumed to be adiabatic. The blind consists of a set of curved louvers with pitch S, width W_B, and thickness t_B, which can be rotated to angle ϕ. The enclosure is filled with a gas ($Pr = 0.71$) and there is assumed to be no insolation. It should also be noted that the bottom slat of the blind is vertically positioned such that it would "seal off" the flow under the blind, if it could be rotated into the fully closed position ($\phi = 90°$).

The flow is assumed to be steady, laminar, incompressible, and two-dimensional. All thermophysical properties are assumed to be constant, except for fluid density which is treated by means of the Boussinesq approximation. With these assumptions, the dimensionless governing equations for the fluid are:

$$\frac{\partial U}{\partial X} + \frac{\partial V}{\partial Y} = 0 \tag{1}$$

$$Gr^{\frac{1}{2}}\left(U\frac{\partial U}{\partial X} + V\frac{\partial U}{\partial Y}\right) = -\frac{\partial P}{\partial X} + \left(\frac{\partial^2 U}{\partial X^2} + \frac{\partial^2 U}{\partial Y^2}\right) \tag{2}$$

$$Gr^{\frac{1}{2}}\left(U\frac{\partial V}{\partial X} + V\frac{\partial V}{\partial Y}\right) = -\frac{\partial P}{\partial Y} + \left(\frac{\partial^2 V}{\partial X^2} + \frac{\partial^2 V}{\partial Y^2}\right) + Gr^{\frac{1}{2}}T^* \tag{3}$$

$$Gr^{\frac{1}{2}}Pr\left(U\frac{\partial T^*}{\partial X} + V\frac{\partial T^*}{\partial Y}\right) = \left(\frac{\partial^2 T^*}{\partial X^2} + \frac{\partial^2 T^*}{\partial Y^2}\right) \tag{4}$$

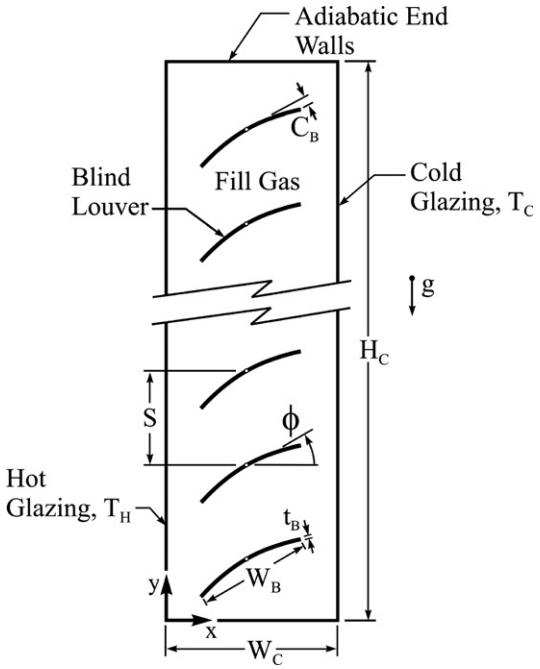

Fig. 1. Model geometry and coordinate system.

where

$$Pr = \frac{c_p\mu}{k_f}, \quad Gr = \frac{g\beta(T_H - T_C)W_C^3\rho^2}{\mu^2} \tag{5}$$

Eqs. (1)–(4) have been cast into dimensionless form using the following dimensionless variables:

$$X = \frac{x}{W_C}, \quad Y = \frac{y}{W_C}, \quad U = \frac{uW_C}{\alpha PrGr^{1/2}}, \quad V = \frac{vW_C}{\alpha PrGr^{1/2}} \tag{6}$$

$$P = \frac{pW_C^2}{\mu\alpha PrGr^{1/2}} \quad T^* = \frac{T - T_C}{T_H - T_C} \tag{7}$$

The conjugate steady conduction in the blind slats has also been included. In these solid regions, the temperature field is given by:

$$\frac{\partial^2 T^*}{\partial X^2} + \frac{\partial^2 T^*}{\partial Y^2} = 0 \tag{8}$$

In this study, two different "classes" of numerical solution have been obtained. The bulk of the data, and the empirical correlation presented later in this paper, have been obtained by solving Eqs. (1)–(4) neglecting the effect of thermal radiation, but including the conjugate conduction in the blind slats. This CFD solution will be referred to as the "*convection-only solution*". The justification for this approximation will be discussed in detail, later in this paper.

In some cases, it was necessary to solve the governing equations including the coupled effects of long-wave radiation. This will be referred to as the "*full solution*". This class of solution was used for validating the numerical solution against experimental data. In the full solution, gray-diffuse radiation exchange has been calculated with the assumption that the fill gas is a non-participating medium. For an enclosure consisting of N surfaces, the radiosity of the kth surface (J_k) can be expressed in terms of the radiosity of the other N surfaces as follows [21]:

$$J_k = \varepsilon_k\sigma T_k^4 + (1 - \varepsilon_k)\sum_{j=1}^{N} F_{kj}J_j \tag{9}$$

where ε_k is the hemispherical emissivity of surface k and F_{kj} is the view factor from surface k to surface j. Eq. (9) represents N equations for the N surface radiosities, which must be solved simultaneously, coupled to the convection and blind conduction.

The governing equations have been solved using the general purpose CFD software FLUENT. The numerical method was based on the control-volume formulation with the SIMPLEC algorithm [22] and a second-order upwind scheme for evaluation of the convective terms.

Results are presented in terms of the local and average Nusselt numbers, defined as follows:

$$Nu_{W_C} = \frac{hW_C}{k_f} = \frac{q''W_C}{k_f(T_H - T_C)},$$

$$\overline{Nu}_{W_C} = \frac{\bar{h}W_C}{k_f} = \frac{qW_C}{k_fH_C(T_H - T_C)} \tag{10}$$

where q'' is the local surface convective heat flux and q is the total surface convective heat transfer rate per unit depth.

3. Grid studies

Extensive testing was done to ensure that the numerical results were grid independent. Also, care was taken to ensure that iterative convergence had been achieved. Iterations were stopped when the normalized residuals of the continuity, momentum and energy equations were reduced to less than 10^{-3}. Convergence of the average Nusselt number was also monitored. Table 1 shows a set of sample results from grid testing for a slat angle of $\phi = 0°$. This table shows near worst-case conditions in terms of grid sensitivity, which occurred at high Rayleigh number and at high values of the blind to enclosure width ratio (W_B/W_C). Grid tests were also undertaken for slat angles of $\phi = 45°$ and 75°. Also, additional tests have been conducted for the "full solution" to ensure that the number of radiation sub-surfaces was sufficient. More details on the numerical solution and grid testing are given in the thesis by Avedissian [23]. Based on these tests, the remainder of the data were obtained using a dimensionless grid size of between 0.015 and 0.025. In all cases, the average Nusselt number data are estimated to be grid independent to better than 1%.

Table 1
Sample grid sensitivity study for the convection-only solution for $\phi = 0°$, $Ra_{W_C} = 10^4$, $W_B/W_C = 0.9$, $A = H_C/W_C = 20$, $k_B/k_f = 4600$

Avg. dimensionless grid size (ΔX, ΔY)	Number of control volumes	$\overline{Nu}_{W_C}$
0.02	50,592	2.785
0.015	91,767	2.832
0.01	202,606	2.840
0.0075	360,045	2.840

4. Comparison with experimental data

The results of the numerical simulations have been compared to some recently published experimental measurements made using a laser interferometer by Naylor and Lai [15]. For these comparisons, the full solution has been used (including conjugate radiation effects). In this numerical model the experimental geometry, surface temperatures, and surface emissivities were matched to those given in the thesis by Lai [24].

Fig. 2 shows a comparison of the numerically predicted temperature field with an infinite fringe interferogram for a slat angle of $\phi = 0°$, $W_B/W_C = 0.862$, and $Ra_{W_C} = 4.6 \times 10^4$. This figure shows the entire enclosure, as well as close-up views of the top and bottom sections. The predicted stream function contours are also shown. It can be

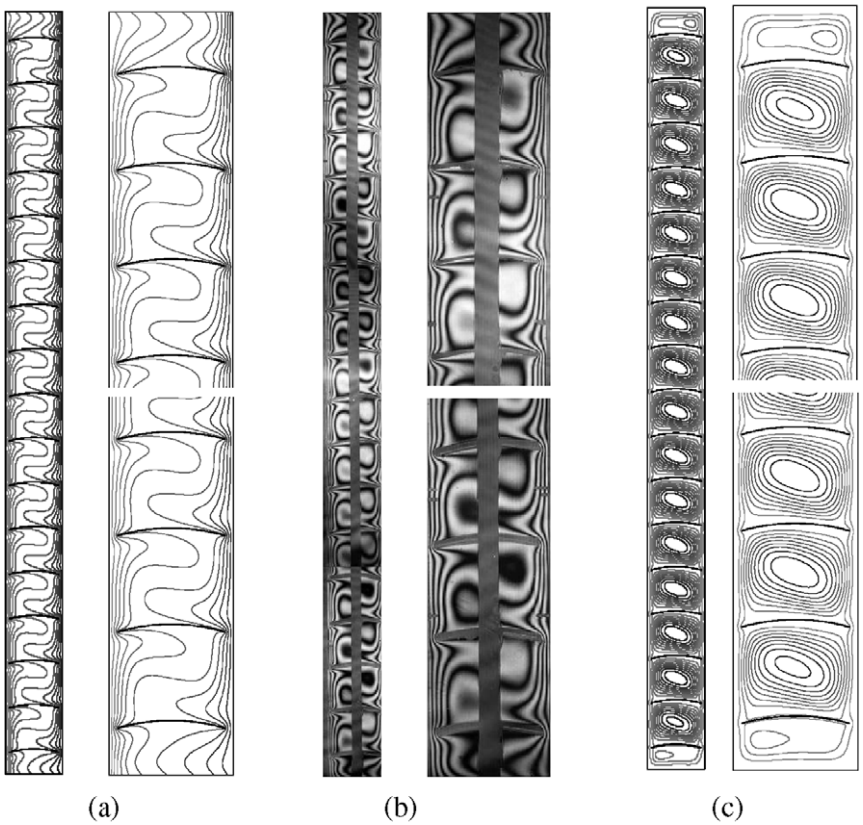

Fig. 2. Comparison of (a) the numerically predicted temperature field, (b) the infinite fringe interferogram of Naylor and Lai [15], and (c) the numerically predicted stream function contours, for a slat angle of $\phi = 0°$ ($Ra_{W_C} = 4.6 \times 10^4$, $A = 13.25$, $W_B/W_C = 0.862$, $k_B/k_f = 4620$, $\varepsilon_B = \varepsilon_H = \varepsilon_C = 0.81$).

seen that, qualitatively, the numerical and experimental temperature fields compare well, both showing a high degree of spatial periodicity.

Fig. 3 shows the local Nusselt number distribution along the hot wall of the enclosure, corresponding to the images shown in Fig. 2. A sketch of the slat positions is shown at the bottom of the graph. It can be seen that the local Nusselt number has a strong periodic variation, with a spatial frequency equal to the slat pitch. High peaks in convective heat transfer rate occur close to the y-locations of the slat tips. These peaks are caused primarily by the "thermal bridging" effect of the aluminum blind, which can be seen clearly in the temperature contours (Fig. 2a and b). In this experiment, the slat tips were in close proximity to the enclosure surfaces (a nominal gap of 2 mm), causing high local heat conduction rates. Overall, it can be seen that the numerical Nu_{W_C} distribution shows good quantitative agreement with the experimental data—the experiment being slightly lower than the numerical predictions, in general. The average Nusselt numbers differ by about 5%, which is within the stated experimental uncertainty (±7%). Also, to some extent, differences in the peak values of Nu_{W_C} near the slat tips can be attributed to imperfections in the fabrication of the experimental model. It was found by Lai [24] that small variations in the glazing-to-tip spacings can cause large variations in the local Nusselt number at these locations. In addition, some differences can be expected close to the top and bottom of the enclosure; in experiment, the acrylic end walls would not have been adiabatic, as assumed in the numerical model. So, overall, the comparisons shown in Figs. 2 and 3 give confidence in the current numerical solution.

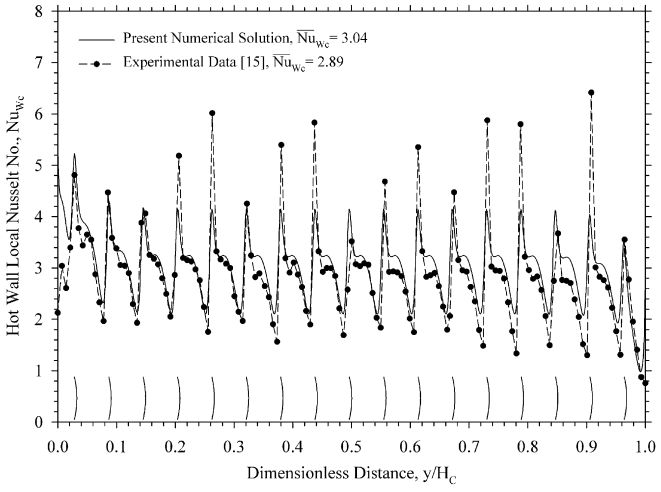

Fig. 3. Comparison of the numerical local Nusselt number distribution on the hot wall with the experimental data of Naylor and Lai [15] for $\phi = 0°$ ($Ra_{W_C} = 4.6 \times 10^4$, $A = 13.25$, $W_B/W_C = 0.862$, $k_B/k_f = 4620$, $\varepsilon_B = \varepsilon_H = \varepsilon_C = 0.81$).

In surprising contrast, the experimental and numerical results for $\phi = 45°$ do not show such close agreement (for $W_B/W_C = 0.862$, $Ra_{W_C} = 4.6 \times 10^4$). Fig. 4 shows the

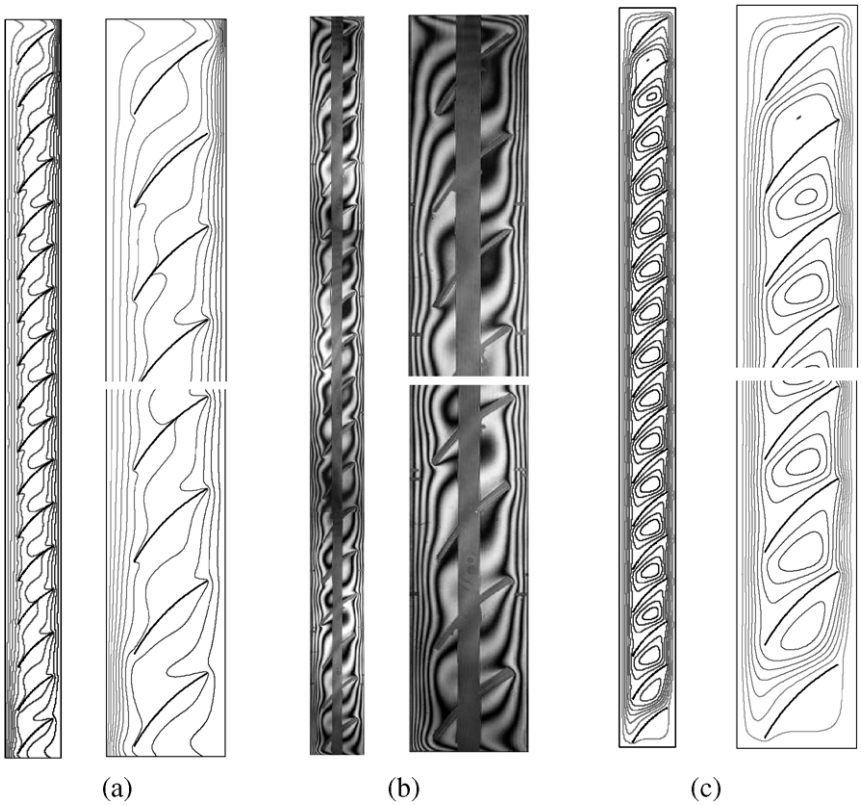

Fig. 4. Comparison of (a) the numerically predicted temperature field, (b) the infinite fringe interferogram of Naylor and Lai [15], and (c) the numerically predicted stream function contours, for a slat angle of $\phi = 45°$ ($Ra_{W_C} = 4.6 \times 10^4$, $A = 13.25$, $W_B/W_C = 0.862$, $k_B/k_f = 4620$, $\varepsilon_B = \varepsilon_H = \varepsilon_C = 0.81$).

predicted temperature field compared to the infinite fringe interferogram. The corresponding hot wall local Nusselt number distributions are shown in Fig. 5. It can be seen that the measured local Nu_{W_C} distribution has much more spatial variation than is predicted numerically. Although the average heat transfer rates are within 10%, Fig. 4 shows a noticeable difference in the predicted temperature fields. It appears from the interferogram that the recirculating flow between the blind slats is stronger than is predicted numerically. The cause of the disagreement is currently unknown. One reason could be that the flow is slightly unsteady for this configuration. The Rayleigh number is quite high from the perspective of a window application. And, at this slat angle, there is a strong flow around the perimeter of the enclosure which might be unstable. Although no unsteadiness was reported during the experiment, it is possible that it was not noticed because of the beam-averaging nature of interferometry. Beam-averaging of the temperature field tends to mask temporal fluctuations, especially those which are not in phase along the path of the laser. Additional research is needed to investigate this discrepancy.

Based on the above comparison, it appears that the current steady/laminar numerical model slightly under predicts the convective heat transfer rate at high Rayleigh number, when the slats are rotated to allow strong convective flow in the enclosure. However, the error in average Nusselt number appears to be only about 10% at $Ra_{W_C} = 4.6 \times 10^4$. It should be noted that this is only a rough estimate, since the uncertainty in the average Nusselt number from interferometric experiment is about ±7%.

The numerical model has also been compared to the overall thermal resistance measurements of Huang [14], which were made using a guarded heater plate (GHP) apparatus. A detailed description of the GHP apparatus is given by Wright and Sullivan [25]. Fig. 6 shows a comparison of the numerically predicted U-value with the experimental results over a range of slat angles at a Rayleigh number of $Ra_{W_C} = 1.4 \times 10^4$. It should be mentioned that these U-values include the effect of typical film coefficients on the indoor and outdoor glazing surfaces, which Huang assumed to be $\bar{h}_o = 23\ \mathrm{W/m^2\,K}$ and $\bar{h}_i = 8\ \mathrm{W/m^2\,K}$. So, for the sake of direct comparison to Huang's measurements, the current numerical results have been adjusted to included these additional thermal resistances, along with the small additional resistance of the two glass panes ($0.0062\ \mathrm{K\,m^2/W}$). With these corrections, the present numerical results are within 3% of Huang's measurements, which is the reproducibility level of the experiment. The third curve in Fig. 6 is the simplified model, which will be discussed later in this paper. It is interesting to note that the actual experimental uncertainty in the individual U-values was reported to be better than ±1%. However, it has been found that the measured U-value can vary by about ±3% from test to test, because of slight variations in the precise horizontal and angular positioning of the individual slats [26].

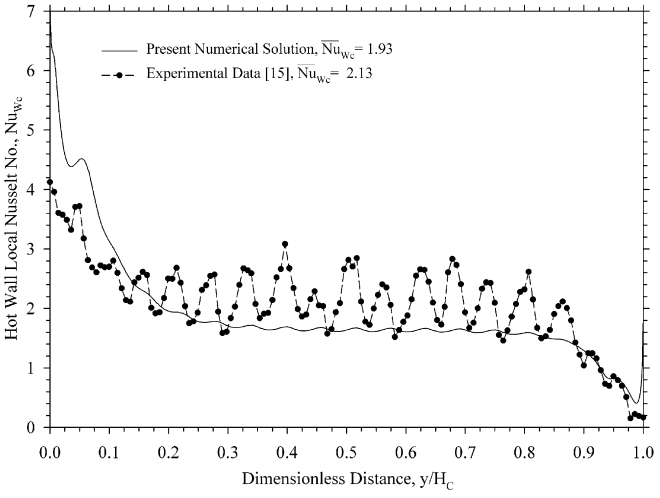

Fig. 5. Comparison of the numerical local Nusselt number distribution on the hot wall with the experimental data of Naylor and Lai [15] for $\phi = 45°$ ($Ra_{W_C} = 4.6 \times 10^4$, $A = 13.25$, $W_B/W_C = 0.862$, $k_B/k_f = 4620$, $\varepsilon_B = \varepsilon_H = \varepsilon_C = 0.81$).

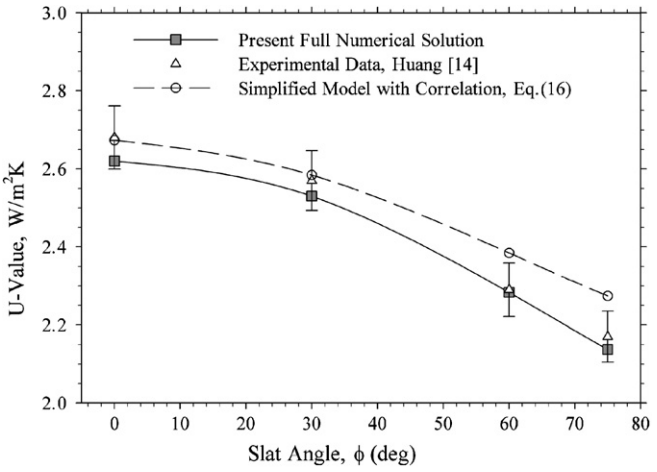

Fig. 6. Comparison of the predicted U-values with the experimental data of Huang [14] from $\phi = 0°$ to $\phi = 75°$ ($Ra_{W_C} = 1.4 \times 10^4$, $T_H \approx 303$ K, $T_H - T_C = 10$ °C (nominal) $\varepsilon_H = \varepsilon_C = 0.84$, $\varepsilon_B = 792$, $W_B/W_C = 0.582$, $A = 23.8$).

5. Results from the numerical parametric study

Data have been obtained from the convection-only numerical solution over the following range of variables:

$$10^2 \leqslant Ra_{W_C} \leqslant 10^5$$
$$W_B/W_C = 0.5, 0.65, 0.8, 0.9$$
$$\phi = 0°, \pm 45°, 75°$$
$$A = H_C/W_C = 20, 40, 60, 100$$

All results were obtained for a blind to fluid conductivity ratio of $k_B/k_f = 4600$, which corresponds approximately to a painted aluminum blind with air as the fill gas. The Prandtl number was fixed at $Pr = 0.71$, which corresponds to typical fill gases (air, argon, krypton) used in window

applications. Blind thickness, curvature, and pitch were set at a constant fraction of the blind width: $t_B = 0.0075W_B$, $C_B = 0.075W_B$, $S = 0.875W_B$. These values were based on measurements made of commercial blinds. Note that the slats in many commercial louvered blinds cannot be rotated beyond $\phi \approx 75°$ because of interference with the slat support mechanism. So, $\phi = 75°$ represents a typical "closed position" for a blind.

The detailed results and a full discussion of the parametric study can be found in the thesis by Avedissian [23]. Only a sample of results will be presented in this paper to illustrate some of the major effects that are at play.

First, it should be noted that numerical results were obtained for slat angles of both $\phi = +45°$ and $\phi = -45°$. However, the average Nusselt numbers for these two cases were always within 1.0%. So, only results for $\phi = +45°$ will be presented.

Fig. 7 shows the effect of the dimensionless blind width (W_B/W_C) on the average Nusselt number over the full range of Rayleigh number considered. Fig. 7a shows results for the slats in the open position, $\phi = 0°$. Fig. 7b shows results for the slats in the closed position, $\phi = 75°$. Also shown in these graphs is the average Nusselt number for a tall enclosure of the same aspect ratio without an internal blind. This "No blind" case was calculated using the empirical correlation of Wright [27].

It can be seen that when the blind is open, the dimensionless blind width has a strong effect on the average convective heat transfer rate. At low Rayleigh number, where the heat transfer is almost by pure conduction, the strong thermal bridging effect of the aluminum slats can be seen clearly. At $W_B/W_C = 0.9$, the heat transfer rate is almost two and a half times greater than for an empty enclosure, because of conduction through the high conductivity slats. As would be expected, this effect decreases as the W_B/W_C ratio decreases. Nevertheless, at low Rayleigh number, the presence of the blind always increases the convective heat transfer rate relative to the "No blind" case. At high Rayleigh number, it can be seen that the blind plays a role in inhibiting the development of convection within the enclosure. For low values of W_B/W_C, the convective heat transfer rate is lower than for the "No blind" case, despite the thermal bridging effect of the horizontal slats.

When the blind is in the closed position ($\phi = 75°$) it can be seen in Fig. 7b that the effect of the dimensionless blind width is small. The effect is small because, in the closed position, the thermal bridging of the blind is greatly reduced. It is interesting to note that in the closed position at high Rayleigh number, the convective heat transfer rate is consistently lower than for the "No blind" case—in this position, the blind significantly reduces the strength of the convection within the enclosure.

Fig. 8 shows the effect of slat angle (ϕ) on the average Nusselt number over the range of Rayleigh numbers studied. Although this graph is for a dimensionless blind width of $W_B/W_C = 0.8$, the results for all values of W_B/W_C were found to have a similar general behavior. At low Rayleigh number, in the conduction regime, increasing the blind angle decreases the average Nusselt number because of the reduced thermal bridging of the blind. This is similar to the effect of decreasing W_B/W_C, previously seen in

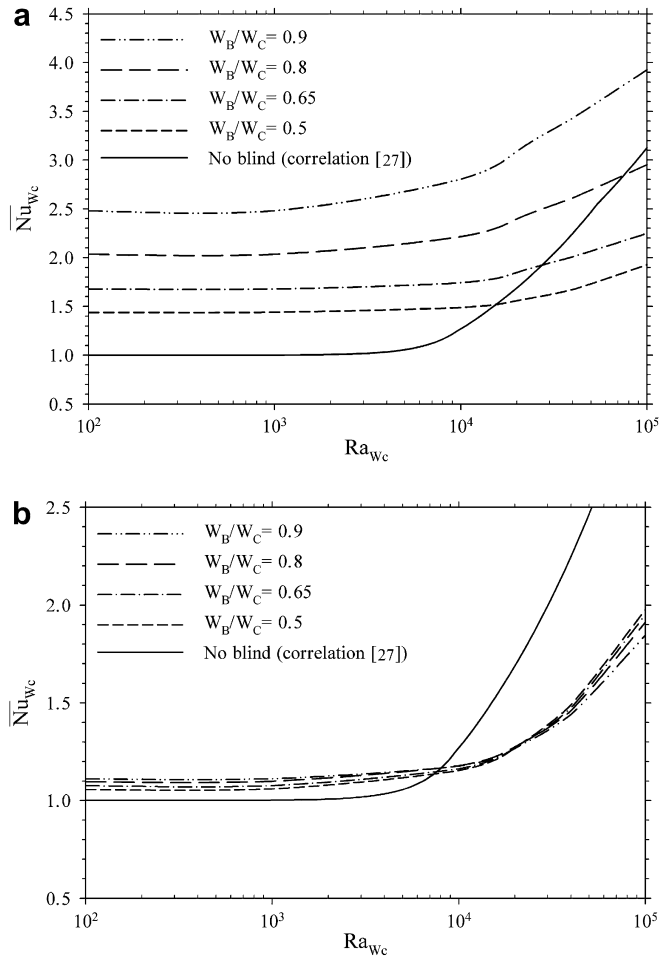

Fig. 7. Effect of dimensionless blind width (W_B/W_C) on the average Nusselt number for (a) $\phi = 0°$ and (b) $\phi = 75°$ ($A = 60$).

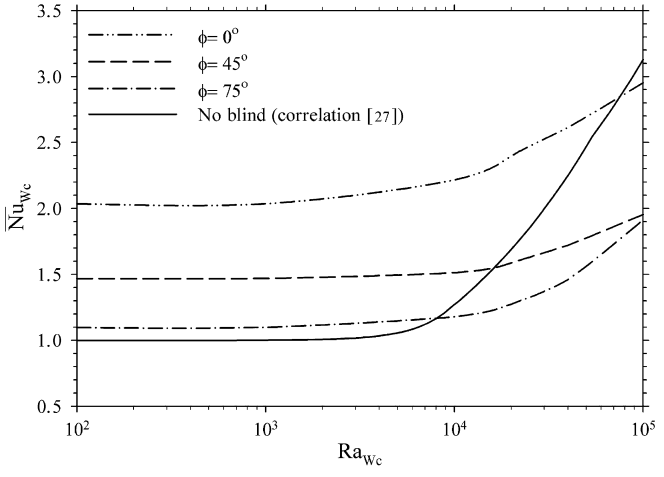

Fig. 8. Effect of slat angle (ϕ) on the average Nusselt number for $W_B/W_C = 0.8$ ($A = 60$).

Fig. 7a. At this particular spacing ($W_B/W_C = 0.8$), the Nusselt number is consistently lower than for the "No blind" case at $Ra_{W_C} = 10^5$. But, in general, whether the convective heat transfer rate is lower or higher than the "No blind" case depends on the trade-off between the thermal bridging and flow inhibiting effects of the blind.

The effect of the enclosure aspect ratio ($A = H_C/W_C$) is shown in Fig. 9. Fig. 9a shows the geometry where the convection is most sensitive to the enclosure aspect ratio. This occurs for the smallest W_B/W_C ratio, when the blind is in the closed position ($\phi = 75°$). In this case, at high Rayleigh number, boundary layers develop on the hot wall, cold wall, and the blind. Hence, the convective heat transfer depends on the vertical extent of these surfaces. As might be expected for this type of flow, the average Nusselt number decreases as the enclosure aspect ratio increases.

In stark contrast, Fig. 9b shows the geometry where the convection is the least sensitive to the enclosure aspect ratio. This occurs when for the largest W_B/W_C ratio, when the blind is in the open position ($\phi = 0°$). For this geometry, at all aspect ratios studied ($A = 20$, 40, 60, 100), the average Nusselt number is essentially unaffected by aspect ratio. This is because there is very little flow around the perimeter of the enclosure. Similar to Fig. 2, the main flow occurs in the space between the slats. The flow and temperature fields are highly periodic. Hence, the convective heat transfer is almost independent of the aspect ratio.

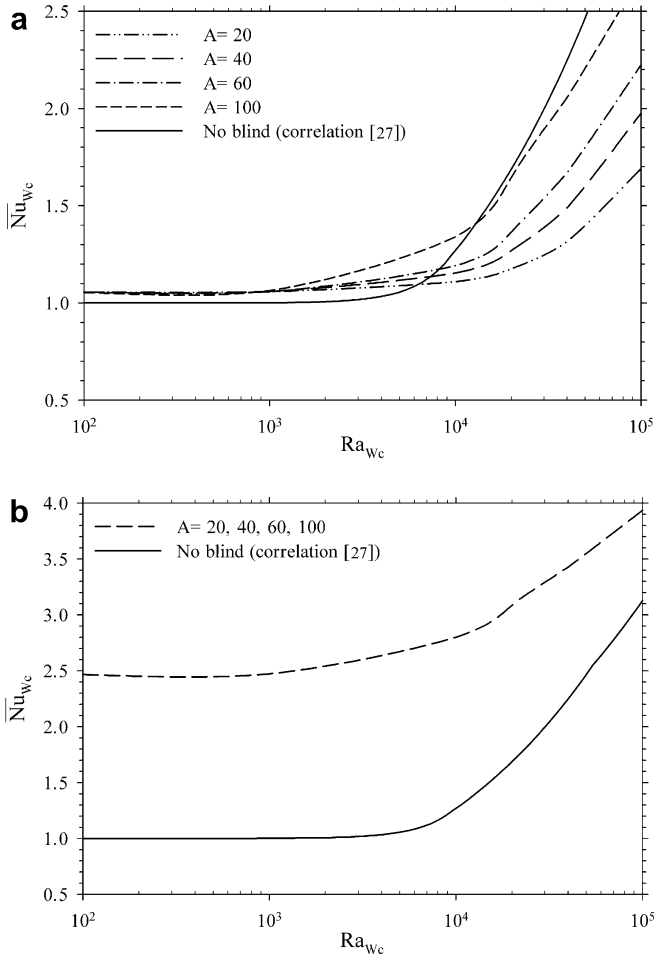

Fig. 9. Effect of enclosure aspect ratio ($A = H_C/W_C$) on the average Nusselt number for (a) $W_B/W_C = 0.5$ and $\phi = 75°$, (b) $W_B/W_C = 0.9$ and $\phi = 0°$.

6. Empirical correlation

The average Nusselt number data from the parametric study have been used to develop an empirical correlation. At moderate and high Rayleigh number it was noted that there are two primary flow patterns inside the enclosure. There is an "outer recirculation" around the perimeter of the enclosure and an "inner recirculation" between the blind slats. The outer recirculation occurs in the gaps between the slat tips and the glazings. These "outer" gaps have a total width in the x-direction of:

$$W_{out} = W_C - W_B \cos(\phi) \tag{11}$$

The inner recirculation occurs in a space that has a nominal width in the x-direction of:

$$W_{in} = W_B \cos(\phi) \tag{12}$$

So, an effective enclosure width (W^*) has been defined using a cubic blend of these two widths, as follows:

$$W^{*3} = B(W_{in})^3 + (1-B)W_{out}^3 = 0.257[W_B\cos(\phi)]^3 + 0.743[W_C - W_B\cos(\phi)]^3 \tag{13}$$

where B is an adjustable constant ($B = 0.257$) that was calculated by least squares minimization. The effective Rayleigh number is based on this blended dimension:

$$Ra_{W^*} = Gr_{W^*}Pr = \frac{g\beta(T_H - T_C)(W^*)^3\rho^2}{\mu^2}Pr \tag{14}$$

In the conduction regime, the average Nusselt number has been correlated as follows:

$$(\overline{Nu}_{W_C})_{cond} = \frac{\bar{h}W_C}{k_f} = \frac{1}{1 - 0.65\frac{W_B}{W_C}[\cos(\phi)]^{1.4}} \quad \text{for } Ra_{W*} \leqslant 500 \tag{15}$$

Eq. (15) predicts the average Nusselt number in the conduction regime with a standard deviation of 1.7% and a maximum error of approximately ±3%. In the convection regime, average Nusselt number was correlated as follows:

$$\frac{\overline{Nu}_{W_C}}{(\overline{Nu}_{W_C})_{cond}} = 1 + 5.75\times10^{-4}(Ra_{W^*} - 500)^{(0.765 - 1.39\times10^{-3}A)} \quad \text{for } Ra_{W*} \geqslant 500 \tag{16}$$

This correlation fits all the data for aspect ratios from $A = 20$ to $A = 100$ with a standard deviation of 4.2% and a maximum error of ±12%. Note that the characteristic dimension in the average Nusselt number is W_C (not W^*). Fig. 10 shows a comparison of the empirical correlation (Eqs. (15) and (16)) with all the data from the current numerical study.

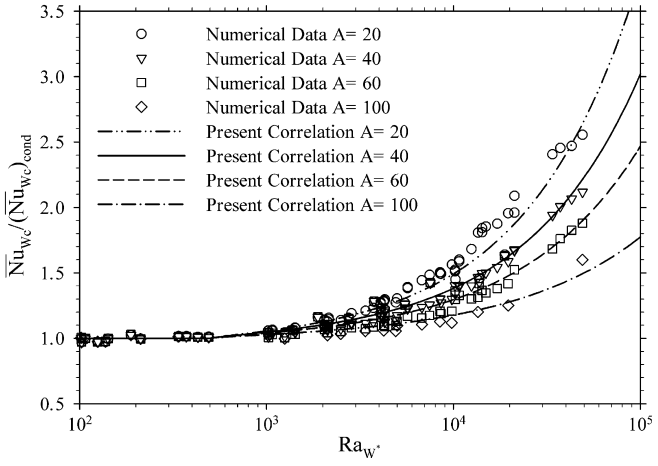

Fig. 10. Comparison of the empirical correlation (Eqs. (15) and (16)) with all the numerical data from the convection-only solution.

It should be noted that this correlation can only be used for a high conductivity blind, i.e., for metal slats. The current study was done for a fixed blind to fluid (gas) conductivity ratio of $k_B/k_f = 4600$. Also, the dimensionless blind thickness was fixed at $t_B/W_B = 0.0075$. So, the dimensionless axial thermal resistance of the blind was held constant at:

$$\frac{W_B k_f}{t_B k_B} = 0.029 \tag{17}$$

Although the results were obtained at this specific value, it is helpful to note that the average Nusselt number is highly insensitive to the axial thermal resistance of the slats, since the dominant thermal resistance is (by far) due to the gas. Numerical testing has been done for the most sensitive case, i.e. the case with the highest levels of thermal bridging by the slats ($Ra_{W_C} = 100$, $W_B/W_C = 0.9$, $\phi = 0°$). For this worst case, it was found that decreasing the axial thermal resistance of the blind by factor of 10 increased the average Nusselt number by only 1.3%. So, in practical terms, the present correlation equation can be used for any value of $W_B k_f/t_B k_B$ lower than 0.029, with only minor error.

When the thermal resistance of the blind was increased, the Nusselt number was somewhat more sensitive. It was found that the current results can be applied for blind/fluid combinations as high as $W_B k_f/t_B k_B = 0.15$, with less than 5% error. This resistance is *five times higher* than the value used in the parametric study. So, the correlation equations are generally applicable to a wide range of fill gases and metal slats, provided $W_B k_f/t_B k_B \leqslant 0.15$.

7. *U*-values predicted using a simplified model

As previously discussed, the parametric study was done using the convection-only numerical solution which neglects the effects of thermal radiation. Since radiation, convection, and conduction are strongly coupled, it is reasonable to question the utility of these results and the empirical correlation that is based on these data. The following discussion addresses this critical issue.

First, it should be recognized that even in a double glazed window *without* an internal blind, the radiative and convective heat transfer rates are strongly coupled. However, if one neglects end-wall effects, this coupling occurs only through the glazing surface temperatures. So, for given surface temperatures, the buoyancy-driven convection can be calculated from the Grashof and Prandtl number, independently of the radiative heat exchange. This means that, although the coupling exists, the enclosure Nusselt number correlation does not have to include the effects of surface emissivities nor absolute surface temperatures. Indeed, this method is used commonly by 1-D window thermal analysis programs, such as WINDOW and VISION.

Naylor and Collins [28] have recently shown that a similar approach can be used to "decouple" the calculation of radiation and convection for the present problem. However, for a double glazed window with a between-panes blind, there is an additional source of coupling between convection and radiation due to the presence of the blind. For example, varying the emissivity of the glazing surfaces will have a strong effect on the steady-state temperature of the blind, which in turn will have a strong influence of the convective heat transfer rates at the glazing surfaces. Fortunately, it has been found that while the convective heat transfer rates depend strongly on the thermal radiation parameters, the convective *resistance* between the blind and the glazings is very weakly coupled to thermal radiation. This result allows the convection coefficient to be obtained from an analysis that neglects radiation. Naylor and Collins [28] have shown that such convection data can be subsequently combined in a simplified 1-D model (with arbitrary values for surface emissivities and absolute glazing temperatures) to obtain the overall *U*-value of the window/blind enclosure. This approach is described briefly below.

Consider a convection coefficient between the hot glazing and the blind ($\bar{h}_{H,B}$) and between the cold glazing and the blind ($\bar{h}_{C,B}$), defined as:

$$q_{conv,H} = \bar{h}_{H,B} H_C (T_H - T_B) \tag{18}$$

$$q_{conv,C} = \bar{h}_{C,B} H_C (T_B - T_C) \tag{19}$$

where $q_{conv,H}$ is the convective heat transfer rate from the hot glazing to the blind and $q_{conv,C}$ is the convective heat transfer rate from the blind to the cold glazing. T_B is the mean blind temperature. For a blind that is located centrally between the glazings, it has been shown that the convective *resistance* divides approximately equally on each side of the blind. Naylor and Collins [28] have shown that $\bar{h}_{H,B}$ and $\bar{h}_{C,B}$ can be closely approximated as:

$$\frac{1}{\bar{h}_{H,B}} = \frac{1}{\bar{h}_{C,B}} = \frac{1}{2\bar{h}_{encl}} \quad \text{or} \quad \bar{h}_{H,B} = \bar{h}_{C,B} = 2\bar{h}_{encl} \tag{20}$$

Table 2
U-value of a double glazed window with a between-panes aluminum blind

Angle ϕ (°)	Hot wall emissivity ε_H	Spacing ratio W_B/W_C	Nominal temp. diff. $T_H - T_C$ (°C)	Ra_{W_C}	Experimental *U*-value [14] (W/m^2/K)	Simplified model *U*-value (W/m^2/K)	Diff. (%)
0	0.84	0.832	20	1.08×10^4	3.08	3.04	−1.4
30	0.84	0.832	20	1.07×10^4	2.86	2.85	−0.5
60	0.84	0.832	20	1.05×10^4	2.54	2.51	−1.0
75	0.84	0.832	20	1.04×10^4	2.32	2.38	+2.7
0	0.164	0.370	10	5.8×10^4	1.61	1.770	+9.9
30	0.164	0.370	10	5.8×10^4	1.63	1.765	+8.3
60	0.164	0.370	10	5.8×10^4	1.63	1.777	+9.0
75	0.164	0.370	10	5.8×10^4	1.63	1.801	+10.5

Comparison of *U*-values predicted by the simplified method compared to experimental data ($T_H \approx 303$ K, $\varepsilon_B = 0.792$, $\varepsilon_C = 0.84$, $W_B = 14.79$ mm, $H_C = 604.5$ mm, $A = 23.8$).

where $1/\bar{h}_{encl}$ is the overall convective resistance between the hot and cold glazings, obtained from the CFD solution that neglects radiation effects i.e., from a convection-only solution. These convective coefficients can be used in a simple energy balance to obtain the blind temperature, as follows:

$$q_{rad,B} = \bar{h}_{H,B} H_C (T_H - T_B) - \bar{h}_{C,B} H_C (T_B - T_C) \quad (21)$$

where $q_{rad,B}$ is the net radiative heat transfer rate from the blind, calculated assuming gray-diffuse radiative heat exchange. In this method, the mean blind temperature is calculated iteratively to satisfy the energy balance (Eq. (21)) for the blind.

Using this 1-D technique, Naylor and Collins [28] have shown that convection coefficients obtained from a CFD solution that excludes the effects of radiation can be subsequently combined with a gray-diffuse radiation model to predict the total thermal resistance of the enclosure with high accuracy. Typically, *U*-values predicted by a full CFD simulation (including radiation) were within 1.5% of the *U*-values predicted by a "convection-only" CFD solution combined with post-processing, using the 1-D energy balance model described above. The current study provides the average Nusselt number correlation of the overall enclosure that is needed to implement this method.

Recently, Collins and Wright [29] have shown that many window analysis programs cannot be used to analyze so-called "diathermanous layers", since they are based on the assumption that all the layers of the window are opaque to long wave radiation. A louvered blind is a diathermanous layer because of its openness. However, it should be noted that the method used in the present *U*-value calculation accounts for long wave radiation exchange directly from glazing to glazing, as well as between the glazings and blind. Hence, when there is no insolation, the current procedure is equivalent to the method of Collins and Wright [29] for treating a diathermanous layer.

As a demonstration, the empirical correlation (Eqs. (15) and (16)) from the present study has been used with the simplified energy balance method of Naylor and Collins [28]. The *U*-values predicted by the simplified method are compared to the measured values of Huang [14] in Table 2, for narrow and wide glazing spacings. Some results are for a regular untreated window ($\varepsilon_H = \varepsilon_C = 0.84$) and some results are for a low emissivity (low-e) coating on the hot glazing ($\varepsilon_H = 0.164$, $\varepsilon_C = 0.84$). The best agreement was obtained for the untreated glass at the narrow glazing spacing ($W_B/W_C = 0.832$). For this case, the agreement is within 3% over the full range of slat angles. It can be seen that the *U*-value is improved when the blind slat is rotated from the open position ($\phi = 0°$) to the closed position ($\phi = 75°$). As the blind is closed, the heat transfer rate decreases because of the reduction in the thermal bridging effect of the aluminum slats, the reduction in convective flow, and the increased radiation shielding provided by the slats.

Now we return to Fig. 6. This figure shows the *U*-value predicted using the current correlation with the data of Huang [14] for a regular double glazed window at an intermediate glazing spacing, $W_B/W_C = 0.582$. In this case, the present empirical correlation predicts the *U*-value within 5% of the experimental measurements.

As shown in Table 2, the poorest agreement was found for a low-e window at the highest glazing spacing ($W_B/W_C = 0.37$). The predicted *U*-value from the one-dimensional model is about 10% higher than the experimental data. For this low-e window, 70–75% of the heat transfer from the inward-facing surface of the hot glazing occurs by convection. So, any error in the convection correlation at high Rayleigh number will be accentuated. It should also be noted that this is an extreme geometry that will be encountered infrequently, if ever, in practical window applications. Also, in some ways this is not a fair comparison, since the numerical data used to develop the average Nusselt number correlation did not consider glazing spacings wider than $W_B/W_C = 0.5$. Nevertheless, the current simplified method shows that for very wide spacings between the blind and glazings, the *U*-value is almost independent of slat angle. This general trend is in agreement with the experimental findings of Huang [14].

8. Conclusion

A numerical study has been conducted of the free convection in an idealized double glazed window with a between-panes louvered metal blind. A parametric study

has been performed of the convection in the enclosure, neglecting the effects of thermal radiation. The convective heat transfer data have been presented in terms of an empirical correlation for the average Nusselt number which is applicable for $Ra_{W_C} \leqslant 10^5$, $20 \leqslant A \leqslant 100$, $0.5 \leqslant W_B/W_C \leqslant 0.9$, $0° \leqslant \phi \leqslant 75°$, $W_B k_f / t_B k_B \leqslant 0.15$. In practice, the limitation of $W_B k_f / t_B k_B \leqslant 0.15$ will restrict the application of the correlation to metal blinds. It has been demonstrated that the correlation can be subsequently combined with a simple one-dimensional energy balance model to predict the *U*-value of the window/blind system for arbitrary radiation parameters. This method is suitable for use in standard window analysis and rating software.

Acknowledgements

This work was funded in part by the Solar Buildings Research Network under the Strategic Network Grants Program of the Natural Sciences and Engineering Research Council of Canada.

References

[1] E.U. Finlayson, D.K. Arasteh, C. Huizenga, M.D. Rubin, M.S. Reilly, WINDOW: Documentation of calculation procedures, Energy and Environmental Division, Lawrence Berkeley Laboratory, Berkeley, CA, USA, 1993.

[2] National Fenestration Rating Council Incorporated, Procedure for determining fenestration product *U*-factors, NFRC 100:2001, Silver Spring, MD, USA, 2002.

[3] Canadian Standards Association, Energy performance of windows and other fenestration systems, Standard A440.2-98, Etobicoke, Ontario, Canada, 1998.

[4] J.L. Wright, H.F. Sullivan, VISION3 Glazing system thermal analysis: Reference manual, Advanced Glazing Laboratory, Department of Mechanical Engineering, University of Waterloo, Waterloo, Ontario, Canada, 1992.

[5] D.S. Yahoda, J.L. Wright, Heat transfer analysis of a between-panes venetian blind using effective longwave radiative properties, ASHRAE Trans. 110 (1) (2004) 455–462.

[6] H. Shahid, D. Naylor, Energy performance of a window with a horizontal venetian blind, Energy Build. 37 (8) (2005) 836–843.

[7] D. Naylor, D.H. Shahid, S.J. Harrison, P.H. Oosthuizen, A simplified method for modeling the effect of blinds on window thermal performance, Int. J. Energy Res. 30 (2006) 471–488.

[8] S.-W. Cho, K.-S. Shin, M. Zaheer-Uddin, The effect of slat angle of windows with venetian blinds on heating and cooling loads of buildings in South Korea, Energy 20 (12) (1995) 1125–1236.

[9] S. Rheault, E. Bilgen, Heat transfer analysis in an automated venetian blind window system, J. Sol. Energy Eng. 111 (1989) 89–95.

[10] M.B. Ullah, G. Lefebvre, Estimation of annual energy-savings contribution of an automated blind system, ASHRAE Trans. 106 (2000) 408–418.

[11] Z. Zhang, A. Bejan, J.L. Lage, Natural convection in a vertical enclosure with permeable screen, J. Heat Transfer 113 (1991) 337–383.

[12] J.M. Garnet, Thermal performance of windows with inter-pane venetian blinds, M.A.Sc. thesis, University of Waterloo, Waterloo, Ontario, Canada, 1999.

[13] R. Dalal, Thermal analysis of a double glazed window with a between-panes pleated blind, M.Eng. Thesis, Ryerson University, Toronto, Ontario, Canada, 2004.

[14] N.Y.-T. Huang, Thermal performance of double glazed windows with inter-pane venetian blinds, Masters Thesis, University of Waterloo, Waterloo, Ontario, Canada, 2005.

[15] D. Naylor, B.Y. Lai, Experimental study of natural convection in a window with a between-panes venetian blind, Exp. Heat Transfer 20 (2007) 1–17.

[16] N. Safer, M. Woloszyn, J.J. Roux, Three-dimensional simulation with a CFD tool of airflow phenomena in a single floor double-skin facade equipped with a venetian blind, Solar Energy 79 (2005) 193–203.

[17] X.D. Fang, A study of the *U*-factor of the window with a high-reflectivity venetian blind, Solar Energy 60 (2) (2000) 207–214.

[18] R. Scozia, R.L. Frederick, Natural convection in slender cavities with multiple fins attached to an active wall, Numer. Heat Transfer, Part A: Appl. 20 (2) (1991) 127–158.

[19] N.A. Kotey, J.L. Wright, Simplified solar optical calculations for windows with venetian blinds, in: Proceedings of the 31st Conference of the Solar Energy Society of Canada, Montreal, Canada, 2006, pp. 1–8.

[20] J.H. Klems, G.O. Kelly, Calorimetric measurements of inward-flowing fraction for complex glazing and shading systems, ASHRAE Trans. 102 (1) (1996) 947–954.

[21] R. Siegel, J.R. Howell, Thermal Radiation Heat Transfer, McGraw-Hill, New York, 1972.

[22] J.P. Van Doormal, G.D. Raithby, Enhancement of the simple method for predicting incompressible flows, Numer. Heat Transfer 7 (1984) 47–163.

[23] T. Avedissian, A numerical study of free convective heat transfer in a double glazed window with a between-pane venetian blind, M.A.Sc Thesis, Ryerson University, Toronto, Ontario, Canada, 2006.

[24] B. Lai, An interferometric study of free convective heat transfer in a double glazed window with a between-panes venetian blind, M.A.Sc Thesis, Ryerson University, Toronto, Ontario, Canada, 2004.

[25] J.L. Wright, H.F. Sullivan, Glazing system *U*-value measurement using a guarded heater plate apparatus, ASHRAE Trans. 94 (2) (1988) 1325–1337.

[26] Personal conversation with Professor J.L. Wright at the Department of Mechanical Engineering, University of Waterloo, Waterloo, Ontario, Canada, February 20, 2004.

[27] J.L. Wright, A correlation to quantify convective heat transfer between vertical window glazings, ASHRAE Trans. 102 (1) (1996) 940–946.

[28] D. Naylor, M.R. Collins, Evaluation of an approximate method for predicting the *U*-value of a window with a between-panes blind, Numer. Heat Transfer, Part A – Appl. 47 (3) (2005) 233–250.

[29] M.R. Collins, J.L. Wright, Calculating performance indices for windows with diathermanous layers, ASHRAE Trans. 112 (2) (2006) 22–29.